Functional Divergence of Human Cytoplasmic Myosin II

KINETIC CHARACTERIZATION OF THE NON-MUSCLE IIA ISOFORM*

Mihály Kovács‡, Fei Wang‡, Aihua Hu, Yue Zhang, and James R. Sellers§

From the Laboratory of Molecular Cardiology, NHLBI, National Institutes of Health, Bethesda, Maryland 20892-1762

Cytoplasmic (or non-muscle) myosin II isoforms are widely expressed molecular motors playing essential cellular roles in cytokinesis and cortical tension maintenance. Two of the three human non-muscle myosin II isoforms (IIA and IIB) have been investigated at the protein level. Transient kinetics of non-muscle myosin IIB showed that this motor has a very high actomyosin ADP affinity and slow ADP release. Here we report the kinetic characterization of the non-muscle myosin IIA isoform. Similar to non-muscle myosin IIB, non-muscle myosin IIA shows high ADP affinity and little enhancement of the ADP release rate by actin. The ADP release rate constant, however, is more than an order of magnitude higher than the steady-state ATPase rate. This implies that non-muscle myosin IIA spends only a small fraction of its ATPase cycle time in strongly actin-bound states, which is in contrast to non-muscle myosin IIB. Non-muscle myosin II isoforms thus appear to have distinct enzymatic properties that may be of importance in carrying out their cellular functions.

Myosin IIs are widespread molecular motors expressed in almost all eukaryotic cell types investigated (1). They share a common domain structure and subunit composition. All myosin II holoenzymes are hexameric with each of the two heavy chains binding an essential and a regulatory light chain. The N-terminal motor domain of the heavy chain contains the nucleotide and actin binding sites and confers ATPase activity. The light chains bind to the neck region. The C-terminal tail domain is responsible for heavy chain dimerization by forming an intermolecular coiled-coil structure. The motor and neck domains constitute the myosin "head" or subfragment-1 (S1).[1]

Some lower eukaryotes such as *Dictyostelium* or *Acanthamoeba* have a single myosin II gene, and thus they are suitable model organisms for genetic studies on the general cellular functions of myosin II (2, 3). In contrast, higher animals express a multitude of myosin IIs. Some of these myosin II isoforms are specific to skeletal, cardiac, or smooth muscle, whereas cytoplasmic or "non-muscle" myosin IIs show ubiqui-

tous tissue distribution. Genomic analysis has revealed the existence of at least three different non-muscle (NM) myosin II isoforms in humans termed NMIIA, NMIIB, and NMIIC (4), of which NMIIA and NMIIB have been investigated at the protein level (5–8). Most tissues contain both NMIIA and NMIIB (9), whereas some cell types are selectively enriched either in NMIIA (such as platelets, lymphocytes, neutrophil granulocytes, brush border cells, RBL2H3 cells) (10) or in NMIIB (neuronal tissue) (11). Little has been published on the localization of NMIIC because this isoform was only recently discovered upon completion of sequencing of the human genome (4).

Detailed transient kinetic studies on several muscle myosin isoforms have provided mechanistic insight into their cyclical interaction with actin and nucleotide that underlies muscle contraction (12–16). Upon ATP binding, the myosin head rapidly detaches from actin and then hydrolyzes ATP. Rebinding to actin is thought to occur in a "primed" conformation of the head with the hydrolysis products at the active site. The subsequent "powerstroke" of the chemomechanical cycle is coupled to product release.

A recent study of the NMIIB isoform showed that, although this myosin uses the same general ATPase mechanism, the unusually low ratio (about 3) of the ADP and phosphate release rate constants and the positive thermodynamic coupling between actin and ADP binding make its working cycle more suited for sustained maintenance of tension, as opposed to short duration force generation that occurs with muscle myosins (8). Therefore, in the light of the partially overlapping localization and the possibility of cofilament formation by the NMIIA and NMIIB isozymes, it is of interest to determine whether NMIIA shares these enzymatic properties. To this end, we performed a transient kinetic characterization of a recombinant NMIIA S1 fragment expressed in the baculovirus/Sf9 cell system. We find that NMIIA S1 exhibits slow kinetics and a high ADP affinity of the actoS1 complex, similarly to NMIIB and smooth muscle myosin. The rate constant of ADP release from actomyosin, however, is about 13 times greater than that of phosphate release. This behavior results in a low duty ratio, which means that only a small fraction of the myosin heads is in strongly actin-bound states at any time during steady-state ATP hydrolysis. NMIIA is therefore similar to smooth and skeletal muscle myosins in this respect, unlike NMIIB, which has an intermediate duty ratio (8, 17). Thus, the two cytoplasmic myosins characterized to date show similar but distinct enzymatic properties.

EXPERIMENTAL PROCEDURES

Cloning, Expression, and Protein Purification—The DNA construct containing the full-length human NMIIA cDNA (MYH9, GenBank accession number M81105) cloned into pBluescript (Stratagene) was created as described previously (7, 18). This plasmid was used as a PCR template to amplify a DNA fragment spanning from the unique *Sfi*I site within the S1 coding region to the 3′-end of NMIIA S1 (amino acid 836) followed by a FLAG tag (DYKDDDDK) coding sequence, a stop codon, and an *Xba*I site.

[1] The abbreviations used are: S1, subfragment-1; mantADP, *N*-methylanthraniloyl-2′-deoxyadenosine 5′-diphosphate; mantATP, *N*-methylanthraniloyl-2′-deoxyadenosine 5′-triphosphate; MDCC-PBP, A197C point mutant bacterial phosphate binding protein labeled with *N*-[2-(1-maleimidyl)ethyl]-7-(diethylamino)coumarin-3-carboxamide; MOPS, 4-morpholinepropanesulfonic acid; NM, non-muscle.

An NMIIA S1 cDNA construct with a C-terminal FLAG tag was created by exchanging this PCR fragment with an *Sfi*I-*Xba*I cassette of the full-length NMIIA cDNA plasmid. The NMIIA S1 cDNA was then subcloned into the baculovirus transfer vector pVL1392 (Invitrogen) between the *Eag*I and *Xba*I sites. The nucleotide sequence of the resulting vector was confirmed by DNA sequencing. The NMIIA S1 heavy chain was coexpressed with essential (bovine non-muscle MLC$_{17B}$) and regulatory (chicken non-muscle MLC$_{20}$) light chains (5). Recombinant baculoviruses were generated, and the expressed protein was purified as described earlier (7).

Actin was prepared from rabbit skeletal muscle according to the method of Spudich and Watt (19). Labeling of actin with pyrene-iodoacetamide was performed as in Ref. 20. Mant nucleotides were purchased from Molecular Probes (Eugene, OR). Other reagents were from Sigma.

Kinetic Experiments—Steady-state ATPase activity was measured using an NADH-coupled assay at 25 °C as described previously (8) in the presence of 10 mM MOPS (pH 7.0), 2 mM MgCl$_2$, 0.15 mM EGTA, and 1 mM ATP. All experiments were performed on unphosphorylated NMIIA S1 because phosphorylation does not affect the steady-state ATPase activity of single-headed smooth muscle and non-muscle myosin constructs (21, 22).

Unless stated otherwise, all stopped flow experiments were carried out in an SF-2001 stopped flow apparatus (KinTek Corp., Austin, TX) at 25 °C in 25 mM MOPS (pH 7.0), 5 mM MgCl$_2$, 100 mM KCl, and 0.1 mM EGTA (for more detailed experimental conditions, see Ref. 8). Phosphate release experiments were performed in 10 mM MOPS (pH 7.0), 2 mM MgCl$_2$, and 0.15 mM EGTA in the SF-2001 instrument essentially as described previously (8) except that two 1-ml syringes were used for the first mix (1:1 volume ratio), which was subsequently pushed alongside a 5-ml syringe containing the third component (1:2.5 mixing ratio), allowing for lower concentrations of actin to be used in the syringe. The performance of the instrument in the double-mixing setup was tested using the reaction of *N*-acetyl-L-tryptophanamide with *N*-bromosuccinimide as well as the binding of inorganic phosphate to MDCC-PBP with the latter having a second order rate constant of about 50 μM^{-1} s^{-1} under our experimental conditions.

Quenched flow experiments were done as described earlier (8) at 25 °C in 25 mM MOPS (pH 7.0), 5 mM MgCl$_2$, and 0.1 mM EGTA.

Data Analysis and Modeling—Concentrations stated in the description of rapid mixing experiments refer to concentrations after mixing unless otherwise indicated. In stopped flow measurements of actin and ADP affinity, equilibrium concentrations *before* mixing are relevant in terms of analyzing amplitudes, whereas the rate parameters are interpreted on the basis of concentrations *after* mixing. Figures and figure legends reflect the actual relevant conditions.
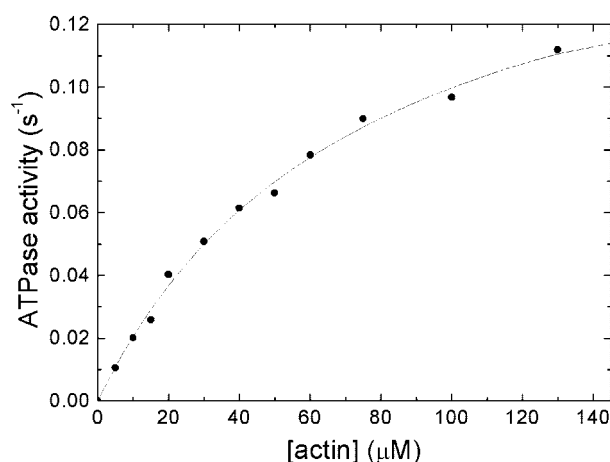
FIG. 1. **Steady-state actin-activated MgATPase activity of NMIIA S1.** Hyperbolic fit of the data yielded a maximal ATPase activity of 0.17 s^{-1} with half-saturation at 75 μM actin in the example shown. The displayed data are corrected for ATPase activities of myosin and actin alone. Conditions: 25 °C, 10 mM MOPS (pH 7.0), 2 mM MgCl$_2$, 0.15 mM EGTA, 1 mM ATP.

chains (5) in the baculovirus/Sf9 expression system. Typically, at least 5 mg of recombinant protein could be prepared from 2×10^9 cells.

We measured the basal and actin-activated MgATPase activity of NMIIA S1 using a NADH-coupled assay at 25 °C in low ionic strength conditions (10 mM MOPS (pH 7.0), 2 mM MgCl$_2$, 0.15 mM EGTA, 1 mM ATP). The basal ATPase activity of NMIIA S1 was 0.013 ± 0.004 s^{-1}, which was activated 13-fold by actin ($V_{max} = 0.17 \pm 0.005$ s^{-1}, Fig. 1). NMIIA S1 had a very high K_{ATPase} of 72 ± 4 μM. Table I summarizes the kinetic parameters of NMIIA S1 and gives a comparison with several other S1 constructs investigated previously.

For practical reasons, we used the same kinetic scheme as was used for NMIIB S1 (8) and other myosins in recent studies (23, 24) (Scheme 1):

$$\text{AM} + \text{ATP} \underset{}{\overset{K_1'}{\rightleftharpoons}} \text{AM(ATP)} \underset{}{\overset{K_2'}{\rightleftharpoons}} \text{AM} \cdot \text{ATP} \underset{}{\overset{K_3'}{\rightleftharpoons}} \text{AM} \cdot \text{ADP} \cdot \text{P}_i \underset{}{\overset{K_4'}{\rightleftharpoons}} \text{AM} \cdot \text{ADP} \underset{}{\overset{K_5'}{\rightleftharpoons}} \text{AM}$$

$$\updownarrow K_6 \qquad \updownarrow K_7 \qquad \updownarrow K_8 \qquad \updownarrow K_9 \qquad \updownarrow K_{10} \qquad \updownarrow K_6$$

$$\text{M} + \text{ATP} \underset{}{\overset{K_1}{\rightleftharpoons}} \text{M(ATP)} \underset{}{\overset{K_2}{\rightleftharpoons}} \text{M} \cdot \text{ATP} \underset{}{\overset{K_3}{\rightleftharpoons}} \text{M} \cdot \text{ADP} \cdot \text{P}_i \underset{}{\overset{K_4}{\rightleftharpoons}} \text{M} \cdot \text{ADP} \underset{}{\overset{K_5}{\rightleftharpoons}} \text{M}$$
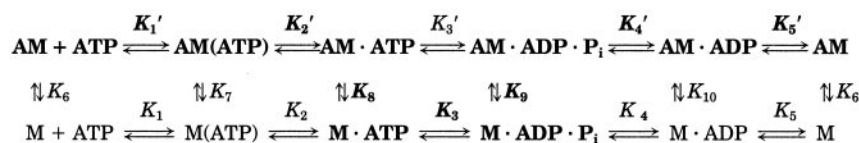
SCHEME 1

Fitting of the experimental data to mathematical functions was done using SigmaPlot 2001 and Origin 5.0 (Microcal Software). In quadratic fits of equilibrium titration curves, constant concentration of the titrated species (*i.e.* pyrene-actin in our experiments) was treated as a floating parameter (just as the maximum amplitude of the signal change) to avoid artifacts arising from uncertainties in concentration determinations and stoichiometry of the components at saturation. Reported standard errors of the mean are those of three separate rounds of experiment, except in some cases (as indicated) where they represent the fitting error of a single data set. Kinetic simulations were performed using Gepasi version 3.21 (©Pedro Mendes, Virginia Bioinformatics Institute).

RESULTS

Protein Design, Expression, and Steady-state ATPase Activity—We expressed a recombinant construct comprising the first 836 amino acids of the NMIIA heavy chain resembling the proteolytic S1 of skeletal muscle myosin. This soluble fragment retains the enzymatic properties of full-length myosin. The heavy chain fragment was coexpressed with recombinant 17-kDa (essential) and 20-kDa (regulatory) light

The numbering of kinetic steps refers to Scheme 1 throughout this paper. The upper line shows the actin-associated pathway of ATP binding, hydrolysis, and product release (AM, actomyosin). The lower line represents the corresponding steps when myosin (M) is dissociated from actin (A). The bold symbols show the main flux pathway of the reaction. Equilibrium constants throughout this paper are expressed as viewed processing to the right on Scheme 1, and those between actin-associated and dissociated states going in the dissociation direction. Rate constants have positive indices in these directions. ATP binding was modeled as a two-step reaction consisting of a second order collision step (K_1 or K_1') and a subsequent isomerization (K_2 or K_2') which becomes rate-limiting at high ATP concentrations. Although ADP binding (and dissociation) has been shown to consist of similar events (25), we consider it as a single step (K_5 or K_5') for simplicity because the substeps were not resolved in the experiments reported herein. The same holds for the ATP hydrolysis step (K_3 or K_3') which has been kinetically resolved to a conformational change and the actual chemical step (26), with phosphate release (K_4 or K_4') probably being similar to it in this respect.

TABLE I

Kinetic parameters of cytoplasmic (non-muscle) and muscle myosin II S1 constructs

Parameter[a]	Signal or calculation in present study	Non-muscle IIA (human)[b]	Non-muscle IIB (human)[c]	Fast skeletal muscle (rabbit)	Cardiac muscle (chicken)	Smooth muscle (chicken)
Steady-state ATPase activity						
Basal (s⁻¹)	NADH assay	0.013 ± 0.004^{d}	0.007^{d}	$0.06^{e,f}$	0.04^{g}	0.06^{g}
V_{max} (s⁻¹)	NADH assay	0.17 ± 0.005^{d}	0.13^{d}	29^{h}	4.2^{i}	0.7^{i}
K_{ATPase} (µM)	NADH assay	72 ± 4^{d}	59^{d}	18^{h}	58^{i}	59^{i}
ATP binding						
$K_1 k_2$ (µM⁻¹ s⁻¹)	MantATP	1.03 ± 0.14	0.65-0.72	$1.8\text{-}2.5^{e,i,j}$	0.5^{i}	$2.1\text{-}3.2^{i,k}$
	Tryptophan	0.56 ± 0.01				
$K_1' k_2'$ (µM⁻¹ s⁻¹)	MantATP	0.14 ± 0.003	0.24-0.40	1.8^{j}	4^{l}	$0.47\text{-}2^{k,l}$
	Pyrene-actin	0.21 ± 0.04				
$1/K_1'$ (µM)	Pyrene-actin	≈ 900	>400	2000^{m}		
k_2' (s⁻¹)	Pyrene-actin	≈ 190	>150	5000^{m}	1500^{l}	1500^{l}
ADP binding						
k_{-5} (µM⁻¹ s⁻¹)	MantADP	0.55 ± 0.06	0.81	$1.4\text{-}1.7^{e,f,n}$		1.1^{k}
k_5 (s⁻¹)	MantADP[o]	0.54 ± 0.23	0.48-0.58	$1.4\text{-}2.5^{i,n}$	2.0^{l}	$0.9\text{-}1.9^{i,k}$
	MantADP[p]	1.12 ± 0.13				
K_5 (µM)	k_5/k_{-5}	1.5 ± 0.4	0.65	2^{k}	0.33^{q}	1.2^{k}
k_{-5}' (µM⁻¹ s⁻¹)	MantADP	2.72 ± 0.16	2.41			
k_5' (s⁻¹)	MantADP[o]	1.72 ± 0.38	0.35-0.38	$>500^{n}$	$>150^{l}$	$15\text{-}22^{h,l}$
	MantADP[p]	2.68 ± 0.30				
K_5' (µM)	k_5'/k_{-5}'	0.8 ± 0.2	0.13	120^{j}	6.7^{q}	5^{k}
	Pyrene-actin[l]	1.4 ± 0.4				
Coupling	K_5'/K_5	0.7	0.2	60	20	
ADP release rate enhancement by actin	k_5'/k_5	2.8	0.7	250	130	12
ATP hydrolysis						
$k_3 + k_{-3}$ (s⁻¹)	Tryptophan	14.1 ± 0.5	17-20	$130^{i,j}$	82^{i}	$40\text{-}50^{i,k}$
	Quenched flow	18.1 ± 2.0				
K_3	Quenched flow	0.61 ± 0.07	0.9	9^{g}		
k_3 (s⁻¹)	$K_3(k_3 + k_{-3})/(1 + K_3)$	7 ± 2	9	120		
k_{-3} (s⁻¹)	k_3/K_3	11 ± 3	10	13		
Phosphate release						
k_4 (s⁻¹)	MDCC-PBP	0.016 ± 0.001^{d}	0.007^{t}			
k_9 (µM⁻¹ s⁻¹)	MDCC-PBP	0.0013 ± 0.0001^{d}	0.0001		0.08^{l}	0.005^{l}
K_9 (µM)	$K_{ATPase}K_3/(1 + K_3)$	27	28	16		
Actin binding						
k_{-6} (µM⁻¹ s⁻¹)	Pyrene-actin	0.73 ± 0.03	0.36		12^{i}	1.24^{k}
K_6 (µM)	Pyrene-actin[r]	<0.01	<0.003	0.033^{k}	0.0063^{q}	0.0035^{k}
k_6 (s⁻¹)	$K_6 k_{-6}$	<0.007	<0.001			
k_{-10} (µM⁻¹ s⁻¹)	Pyrene-actin	0.19 ± 0.02	0.26			0.23^{k}
K_{10} (µM)	Pyrene-actin[r]	≈ 0.02	<0.001	1^{j}	0.1^{q}	0.024^{k}
k_{10} (s⁻¹)	$K_{10} k_{-10}$	≈ 0.004	<0.0003			
Coupling	K_{10}/K_6	≈ 2	≈ 0.4	30	15	4.2

[a] Numbering of steps refers to Scheme 1.

[b] Present study, 25 °C, pH 7, 100 mM KCl, unless stated otherwise. Reported means ± standard errors are those of three different rounds of experiment.

[c] (8), 25 °C, pH 7, 100 mM KCl unless otherwise indicated.

[d] No KCl.

[e] (25), 21 °C, pH 8, 100 mM KCl.

[f] (41), 21 °C, pH 8, 100 mM KCl.

[g] (15), 25 °C, pH 7, no KCl.

[h] (42), 25 °C, pH 8, 30 mM KCl.

[i] (15), 25 °C, pH 7, 10 mM KCl.

[j] (43), 20 °C, pH 7, 100 mM KCl.

[k] (13), 20 °C, pH 7, 100 mM KCl.

[l] (15), 20 °C, pH 7, 10 mM KCl.

[m] (44), predicted.

[n] (45), 20 °C, pH 7, 100 mM KCl.

[o] From the intercept of the k_{obs} *versus* [mantADP] plot.

[p] From ATP chasing experiment.

[q] (16), bovine cardiac S1, 25 °C, pH 7, 100 mM KCl.

[r] From amplitude data.

[s] (46), 22 °C, pH 8, 50 mM KCl.

[t] 50 mM KCl.

ATP Binding and Actomyosin Dissociation—The fluorescent nucleotide, mantATP, shows a fluorescence enhancement on binding to myosin S1. When mixed in the stopped flow apparatus under pseudo-first order conditions (0.1 µM NMIIA S1 and 1–15 µM mantATP), the obtained traces could be fitted to single exponentials. The dependence of the observed rate constant (k_{obs}) on mantATP concentration was linear and gave an apparent second order rate constant ($K_1 k_2$) of 1.03 ± 0.14 µM⁻¹ s⁻¹ (Fig. 2A and Table I). The binding rate constant of mant-

ATP to actoNMIIA S1 ($K_1' k_2'$) appeared to be much slower (0.14 ± 0.003 µM⁻¹ s⁻¹, Fig. 2A), which is in contrast to various muscle myosin isoforms (Table I).

ATP causes dissociation of the complex of NMIIA S1 with pyrene-labeled actin that was accompanied by an increase in pyrene fluorescence. The time course was a single exponential, and the observed rate constant depended hyperbolically on ATP concentration with half-saturation around 900 µM ATP (Fig. 2B). The maximal value of the observed rate constant of
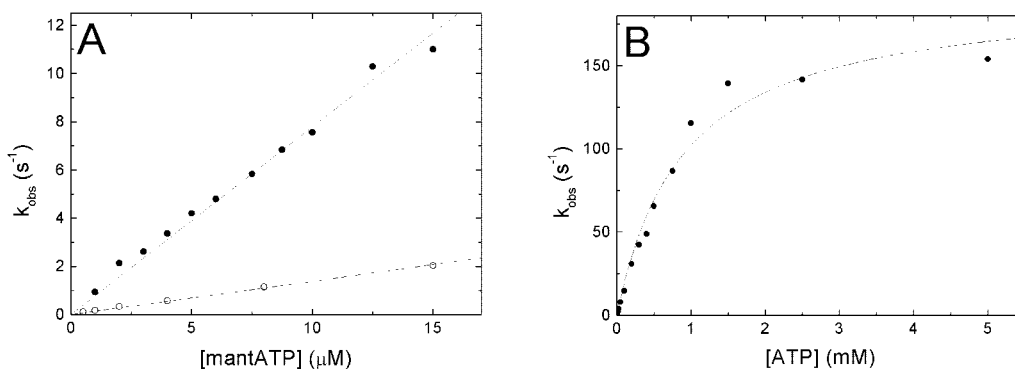
FIG. 2. **ATP binding and ATP-induced actomyosin dissociation in NMIIA S1.** *A*, dependence of the observed pseudo-first order rate constants (k_{obs}) of mantATP binding to 0.1 μM NMIIA S1 (*solid symbols*) or 0.05 μM actoNMIIA S1 (*open symbols*) on mantATP concentration. The slopes of the plots yielded apparent second order rate constants of 0.78 μM^{-1} s^{-1} for NMIIA S1 ($K_1 k_2$) and 0.14 μM^{-1} s^{-1} for actoNMIIA S1 ($K_1' k_2'$) in the experiments shown. *B*, ATP-induced dissociation of the pyrene-actoNMIIA S1 complex (10 nM). Pyrene fluorescence transients were fitted to single exponentials, and the obtained k_{obs} values were plotted against the ATP concentration. Hyperbolic fit to the data yielded a maximal dissociation rate of 190 s^{-1} with half-saturation at 900 μM ATP in the example shown. Conditions: 25 °C, 25 mM MOPS (pH 7.0), 5 mM MgCl$_2$, 100 mM KCl, 0.1 mM EGTA.

dissociation was around 190 s^{-1}, showing that the isomerization step leading to actomyosin dissociation is much slower in NMIIA than other myosins investigated to date except for NMIIB (Table I). A linear fit to the data points at low [ATP] yielded a value of 0.21 $\pm$ 0.04 μM^{-1} s^{-1}, which is similar to the $K_1' k_2'$ value measured with mantATP binding.

ATP Hydrolysis—Upon mixing with ATP in the stopped flow apparatus, an ~5% increase in NMIIA tryptophan fluorescence was detected (Fig. 3A). The fluorescence change was monophasic and yielded an apparent second order rate constant ($K_1 k_2$) of 0.56 $\pm$ 0.01 μM^{-1} s^{-1} at low [ATP], a value about one-half of that seen with mantATP binding (Table I). The k_{obs} showed saturation at 14.1 $\pm$ 0.5 s^{-1} (Fig. 3B), indicating that it is limited by the apparent rate of ATP hydrolysis ($k_3 + k_{-3}$). This assumption was confirmed by quenched flow experiments directly monitoring the breakdown of ATP into products. At 50 μM ATP, a single exponential burst with a k_{obs} of 18.1 $\pm$ 2.0 s^{-1} ($k_3 + k_{-3}$) was followed by a linear steady-state phase of ATP hydrolysis (Fig. 3C). The calculated steady-state ATPase rate was 0.014 s^{-1}, in good agreement with the results of the NADH-coupled assay (see above). In the presence of 20 μM actin, the k_{obs} of the burst phase was slowed down to around 13 s^{-1} at 50 μM ATP (data not shown), consistent with the slow ATP binding rate constant of actoNMIIA S1 (see above), indicating that nucleotide binding is still rate-limiting in these conditions. The rate of the steady-state phase was increased to about 0.05 s^{-1} by 20 μM actin.

The amplitude of the burst phase in the quenched flow experiments was unusually low (values between 0.3 and 0.4 mol of P$_i$/mol of NMIIA S1 were obtained, regardless of the presence of actin), similarly to earlier observations on human NMIIB (8). Because these values are affected by the accuracy of protein concentration measurements and the proportion of nonfunctional protein in the preparation, we carried out single turnover quenched flow experiments to obtain an independent measure of the burst amplitude (Fig. 3D). These measurements confirmed the burst amplitude stated above, indicating that the equilibrium constant of the ATP hydrolysis step on the enzyme (K_3) is as low as 0.61 $\pm$ 0.07 ($K_3 = A/(1 - A)$, where A is the burst amplitude expressed as n(P$_{i\ burst}$)/n(S1$_{total}$) in the multiple turnover experiment, and n(P$_{i\ burst}$)/n(ATP$_{total}$) in single turnover conditions). From the hydrolysis equilibrium constant and the rate constant of the burst at 50 μM ATP, a k_3 value of 7 $\pm$ 2 s^{-1} and a k_{-3} of 11 $\pm$ 3 s^{-1} could be calculated (Table I).

Phosphate Release—The kinetics of phosphate release from NMIIA S1 and actoNMIIA S1 was followed using a fluorescently labeled bacterial phosphate binding protein (MDCC-

PBP) (27). Mixing NMIIA S1 with ATP under single turnover conditions (1.4 μM S1 and 1 μM ATP) resulted in an increase in MDCC-PBP fluorescence with a k_{obs} (= k_4) of 0.016 $\pm$ 0.001 s^{-1}, in good agreement with the results of the steady-state ATPase measurements (see above). P$_i$ release from actoS1 was measured in the sequential mixing mode of the stopped flow apparatus. First, NMIIA S1 and ATP was mixed at a volume ratio of 1:1 to yield an S1 concentration of 1.4 μM and ATP concentration of 1 μM after mixing. This mixture was incubated for 5 s for ATP binding and hydrolysis to occur and then mixed rapidly with actin filaments while monitoring the change in MDCC-PBP fluorescence. Single exponential traces were observed throughout the actin concentration range studied (0–60 μM, Fig. 4, *A* and *B*). The observed phosphate release rate constants showed good agreement with the steady-state ATPase activities at the corresponding actin concentrations (Fig. 4B; *cf*. Fig. 1; note that Fig. 1 is corrected for basal ATPase activity of NMIIA S1, whereas Fig. 4B is not). No sign of saturation was detectable up to 60 μM actin concentration, thus it appears that the actin affinity of the M·ADP·P$_i$ species is very low, and the maximal rate of P$_i$ release from AM·ADP·P$_i$ (k_4') could not be measured directly. A linear fit to the k_{obs} *versus* [actin] plot gave an apparent on-rate constant of 0.0013 $\pm$ 0.0001 μM^{-1} s^{-1} for M·ADP·P$_i$ binding to actin (Fig. 4B and Table I).

A control experiment with skeletal muscle S1 at 20 °C, in which 3.5 μM S1 was incubated with 2 μM ATP for 3 s and then mixed with actin (30 μM final concentration), gave a biphasic phosphate release transient with rate constants of 30 s^{-1} (amplitude: 20%) and 1 s^{-1} (80%), consistent with previous observations described in Ref. 28 (data not shown).

ADP Binding and Affinity—MantADP showed a fluorescence enhancement of magnitude similar to mantATP when binding to NMIIA S1. The k_{obs} of the single exponential transients obtained on binding of mantADP (1–4 μM) to NMIIA S1 (0.1 μM) was linearly dependent on mantADP concentration (Fig. 5A) and gave an apparent second order binding rate constant (k_{-5}) of 0.55 $\pm$ 0.06 μM^{-1} s^{-1}. The intercept of the plot representing the mantADP dissociation rate constant from NMIIA S1 (k_5) was 0.54 $\pm$ 0.23 s^{-1}. When mantADP was mixed with actoNMIIA S1, a k_{-5}' value of 2.72 $\pm$ 0.16 μM^{-1} s^{-1} and an intercept (k_5') of 1.72 $\pm$ 0.38 s^{-1} were obtained. The off-rates were also confirmed by a second experiment, in which NMIIA S1 or actoNMIIA S1 (0.05–0.1 μM) was preincubated with mantADP (0.5–2 μM) and then mixed rapidly with excess (100–200 μM) ATP. In this experiment, the observed rate constant of the decrease in mantADP fluorescence was limited by the mant-
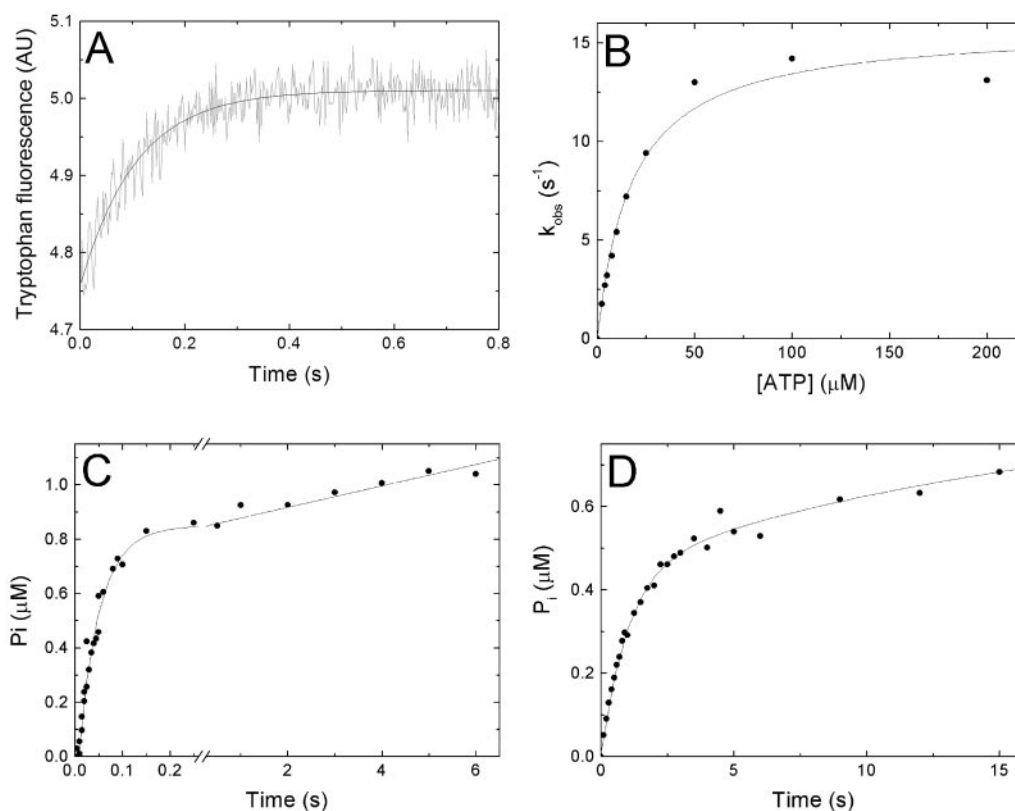
FIG. 3. **Kinetics of ATP hydrolysis by NMIIA S1.** *A*, tryptophan fluorescence enhancement on the reaction of 0.2 μM NMIIA S1 with 25 μM ATP. Excitation was at 295 nm, and emitted light was selected through a band-pass filter centered at 347 nm. Single exponential fit to the data yielded a k_{obs} of 9.3 s^{-1}. *B*, dependence of the observed rate constant of tryptophan fluorescence enhancement on ATP concentration. Hyperbolic fit yielded a maximal k_{obs} of 15.8 s^{-1} with half-saturation at 18 μM ATP in the example shown. *C*, kinetics of ATP hydrolysis measured by quenched flow. Shown is the time course of the reaction of 2.7 μM NMIIA S1 with 50 μM ATP. Data were fit to a single exponential burst with a linear steady-state phase to yield a burst amplitude of 0.91 μM P_i (corresponding to 0.34 mol of $P_{i\ burst}$/mol of NMIIA $S1_{total}$) with a k_{obs} of 20 s^{-1} and a steady-state slope of 0.014 s^{-1} in the example shown. Note the break in the *x* axis. *D*, ATP hydrolysis under single turnover conditions. The reaction of 2.3 μM NMIIA S1 with 1 μM ATP was followed by quenched flow. A double exponential approximation was used to determine the burst amplitude where the k_{obs} of the fast phase of the transient was limited by ATP binding and that of the slow phase by product release. The amplitude of the fast phase was 0.43 μM P_i (corresponding to 0.43 mol of $P_{i\ burst}$/mol of ATP_{total}) in the experiment displayed. Conditions: *A* and *B*, as in Fig. 2; *C* and *D*, 25 °C, 10 mM MOPS (pH 7.0), 2 mM MgCl$_2$, 0.15 mM EGTA. *AU*, arbitrary units.
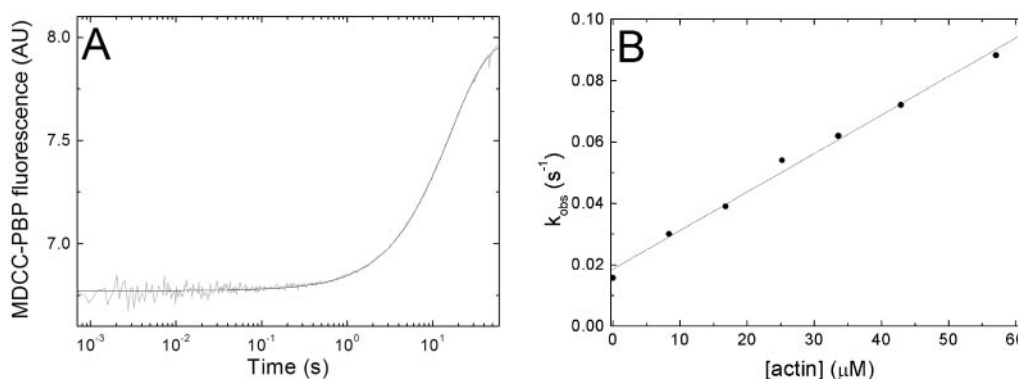
FIG. 4. **Phosphate release from NMIIA S1 and actoNMIIA S1 during single turnovers.** *A*, in the experiment shown, 1.4 μM S1 was mixed with 1 μM ATP (conditions after first mix), incubated for 5 s in a delay line for ATP binding and hydrolysis to occur, and then mixed rapidly with actin to a final actin concentration of 34 μM and a final S1 concentration of 0.4 μM. The observed trace was a single exponential with a k_{obs} of 0.061 s^{-1}. *B*, dependence of the observed rate constant of the phosphate release transients on actin concentration. The obtained values show good agreement with the steady-state ATPase activities. (In Fig. 1, note that steady-state data are corrected for basal myosin ATPase (0.013 s^{-1}), whereas data in this figure are not.) The k_{obs} did not show signs of saturation up to 60 μM actin. Linear fit to the data yielded an apparent on-rate constant of M·ADP·P$_i$ binding to actin of 0.0013 μM^{-1} s^{-1} with an intercept at 0.019 s^{-1} (P_i release rate constant in the absence of actin) in the example shown. Conditions were as in Fig. 3*C*. All syringes contained 1.5 μM MDCC-PBP and a "phosphate mop" (27). *AU*, arbitrary units.

ADP off-rate from NMIIA S1 or actoNMIIA S1 (Fig. 5*B*). The k_{obs} of the observed single exponential transients was 1.12 ± 0.13 s^{-1} in NMIIA S1 (k_5) and 2.68 ± 0.30 s^{-1} in actoNMIIA S1 (k_5'), in agreement with the intercept values mentioned above. These results indicate an ADP affinity of NMIIA S1 ($K_5 = 1.5 ±$ 0.4 μM) similar to other myosin IIs. The ADP affinity, however,

is not weakened by actin ($K_5' = 0.8 ± 0.2$ μM), in striking contrast to muscle myosins (*cf.* Table I).

We verified the surprisingly low K_5' value by an independent measurement, in which 40 nM pyrene-actoNMIIA S1 complex was preincubated with a range of ADP concentrations and then mixed rapidly with 200 μM ATP (premixing concentrations
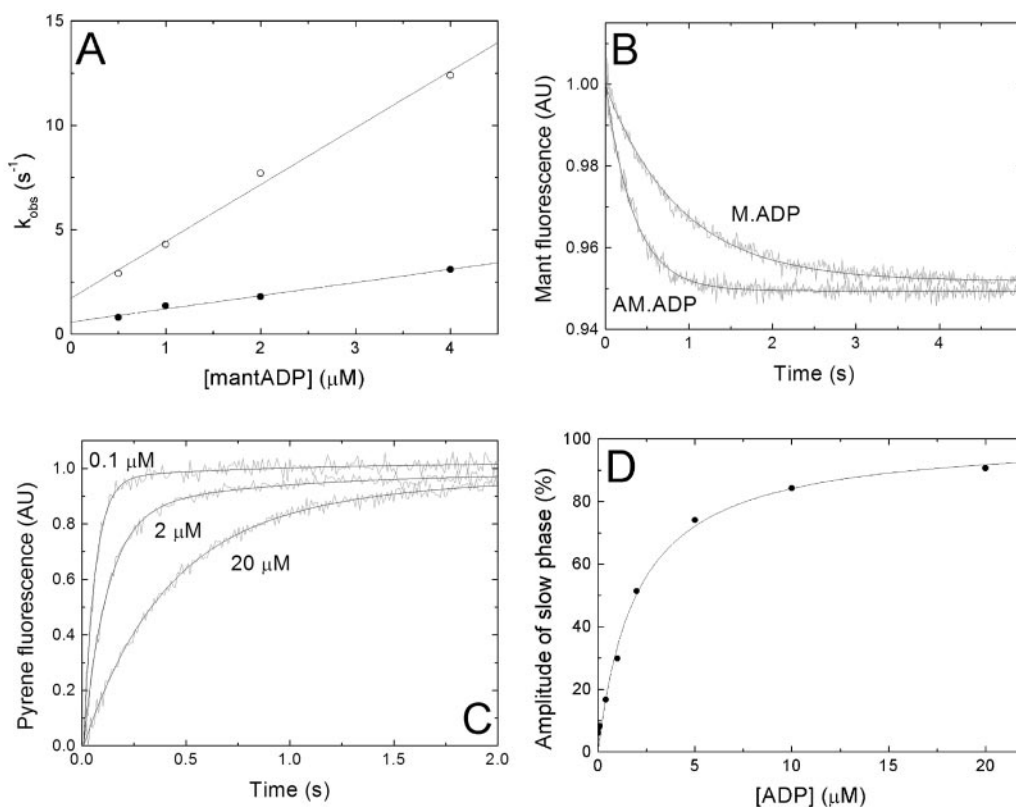
FIG. 5. **ADP binding and affinity.** *A*, mantADP concentration dependence of k_{obs} of the mant fluorescence transients recorded on mantADP binding to 0.1 μM NMIIA S1 (*solid symbols*) or 0.1 μM actoNMIIA S1 (*open symbols*). Linear fit of the data gave an apparent second order binding rate constant of 0.63 μM^{-1} s^{-1} for NMIIA S1 (k_{-5}) and 2.72 μM^{-1} s^{-1} for actoNMIIA S1 (k_{-5}'), whereas the intercepts indicating ADP off-rate constants were 0.58 s^{-1} (k_5) and 1.72 s^{-1} (k_5') for NMIIA S1 and actoNMIIA S1, respectively, in the experiments shown. *B*, mantADP off-rate constants were verified by chasing experiments, in which the M·ADP or AM·ADP complexes were mixed rapidly with excess ATP, and the decrease in mant fluorescence was followed. When 0.05 μM NMIIA S1 and 0.5 μM mantADP were preincubated and then mixed rapidly with 200 μM ATP, the observed rate constant (k_5) was 1.11 s^{-1} in the example shown (M·ADP trace). Similarly, an actoNMIIA.ADP off-rate constant (k_5') of 2.95 s^{-1} was determined by preincubating 0.1 μM actoNMIIA S1 and 2 μM mantADP and then mixing with 100 μM ATP (AM·ADP trace). Data were normalized to the start point of the reaction. *C*, the ADP affinity of actoNMIIA was assessed by preincubating 0.04 μM pyrene-actoNMIIA S1 with a range of ADP concentrations and then mixing rapidly with 200 μM ATP (premixing concentrations stated in this *panel*). Selected traces are shown with the ADP concentrations indicated. The observed pyrene fluorescence transients were double exponential with the fast phase ($k_{obs} \approx 20$ s^{-1}) representing ATP-induced dissociation of actoNMIIA S1 with no bound ADP, whereas the slow phase (k_{obs} ~2–3 s^{-1}) originated from the ADP-bound fraction of actoNMIIA S1, and this process was limited by ADP dissociation from actoNMIIA S1. Data shown are normalized to the start and end points of the transients. *D*, the fractional amplitude of the slow phase ($A_{slow}/(A_{fast} + A_{slow})$) of the transients described in *C* plotted against ADP concentration (premixing concentrations). A hyperbolic fit of the data revealed a K_5' of 2.0 μM in the experiment shown. Conditions were as in Fig. 2. *AU*, arbitrary units.

indicated in this case). The observed pyrene fluorescence transients were biphasic with the amplitude of the fast phase representing the population of free (not ADP-bound) actoNMIIA S1 (with a k_{obs} of ~20 s^{-1}, reflecting the ATP on-rate), whereas the amplitude of the slow phase reflects the abundance of the AM·ADP species ($k_{obs} \approx 2$ s^{-1}, Fig. 5*C*). The dependence of the relative amplitude of the slow phase ($A_{slow}/(A_{fast} + A_{slow})$) on ADP concentration was hyperbolic (Fig. 5*D*) and yielded a K_5' of 1.4 $\pm$ 0.4 μM, corroborating the small value calculated from the on- and off-rate constants.

Actin Interaction—Binding of NMIIA S1 to pyrene-labeled actin filaments caused a quench in pyrene fluorescence. The apparent second order rate constant of actin binding to NMIIA S1 was measured by following the quench upon mixing 0.1 μM NMIIA S1 with a range of pyrene-actin concentrations (1–4 μM) and then plotting the observed rate constants of the transients *versus* pyrene-actin concentration (Fig. 6*A*). A linear fit to the data revealed a k_{-6} of 0.73 $\pm$ 0.03 μM^{-1} s^{-1}. The on-rate constant of pyrene-actin binding to the M·ADP complex ($k_{-10} = 0.19 \pm 0.02$ μM^{-1} s^{-1}) was determined similarly but in the presence of 15 μM ADP (Fig. 6*A*).

The fractional binding of NMIIA S1 to actin was assessed by preincubating 15 nM pyrene-actin with various concentrations of NMIIA S1 and then mixing rapidly with 10 μM ATP (concentrations before mixing) (29). The observed increase in pyrene fluorescence was single exponential with k_{obs} values around 1 s^{-1} (*cf.* $K_1'k_2'$, Table I). The dependence of the observed amplitude of the fluorescence change on NMIIA S1 concentration indicated a high actin affinity of NMIIA S1 (Fig. 6*B*). Throughout the concentration range examined, practically all NMIIA S1 molecules were bound to actin at equilibrium, and K_6 was estimated to be less than 10 nM.

The affinity of NMIIA S1 for actin in the presence of ADP was evaluated in a similar experiment, in which 15 nM pyrene-actin was preincubated with various concentrations of NMIIA S1 and 30 μM ADP and then mixed rapidly with 300 μM ATP (concentrations before mixing). The observed rate constant of pyrene-actoNMIIA S1 dissociation was around 2 s^{-1}, showing that the reaction was limited by ADP dissociation from the AM·ADP complex. Fig. 6*C* shows the dependence of the reaction amplitude on NMIIA S1 concentration. The data, unlike in the absence of ADP, clearly deviated from a hypothetical curve of complete NMIIA S1 binding to actin throughout the examined concentration range. A quadratic fit yielded a dissociation constant (K_{10}) around 20 nM.

Although only the upper limit of K_6 could be determined from
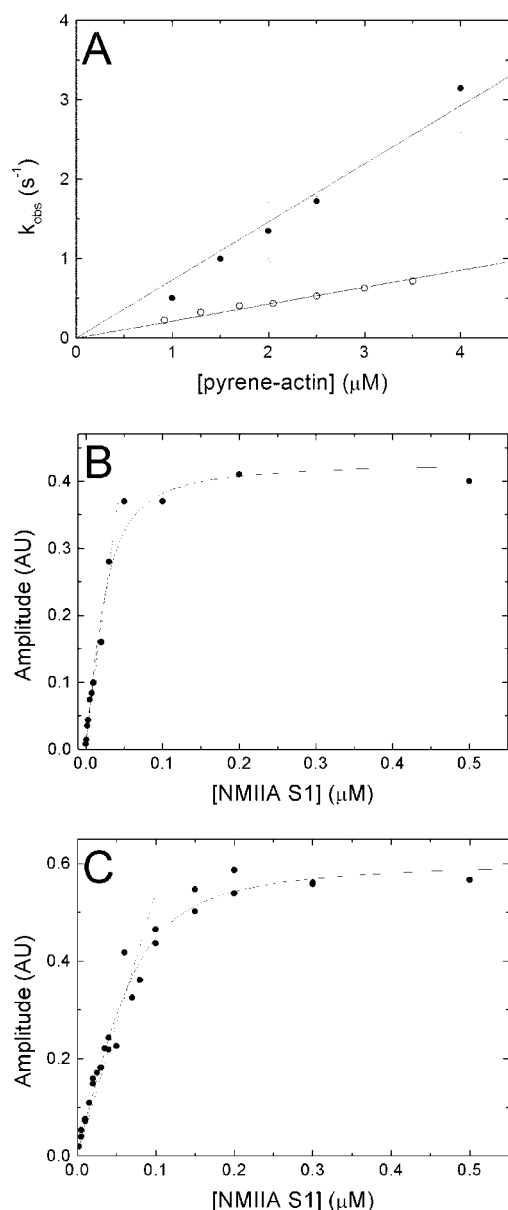
FIG. 6. **Actin interaction.** *A*, dependence of the k_{obs} of the pyrene fluorescence transients recorded on mixing 0.1 μM NMIIA S1 (*solid symbols*) or NMIIA S1·ADP complex (0.1 μM NMIIA S1 plus 15 μM ADP, *open symbols*) with pyrene-actin at different concentrations. Linear fits to the data sets gave 0.73 ± 0.03 μM^{-1} s^{-1} for k_{-6} (average of two experiments) and 0.21 μM^{-1} s^{-1} for k_{-10} (example shown). *B*, the actin affinity of NMIIA S1 was assessed by preincubating 15 nM pyrene-actin with a range of NMIIA S1 concentrations and then mixing rapidly with 10 μM ATP (premixing concentrations stated). A representative data set is shown, in which the amplitude of the pyrene fluorescence increase transients (k_{obs} ∼0.7 s^{-1}) was plotted against the NMIIA S1 concentration. Fitted binding curves with $K_6 = 0$ (*dashed line*) or $K_6 = 10$ nM (*solid line*) as a fixed parameter are shown. The data show that NMIIA S1 has a high affinity for actin ($K_6 < 10$ nM), but they do not allow for more exact determination of K_6. *C*, the affinity of NMIIA S1·ADP for actin was determined in an experiment similar to that in *B* except that 15 nM pyrene-actin plus 30 μM ADP plus NMIIA S1 at various concentrations were preincubated and then mixed with 300 μM ATP (premixing concentrations stated). Amplitudes of the pyrene fluorescence transients ($k_{obs} \approx 2$ s^{-1}) from two rounds of experiment are plotted against the NMIIA S1 concentration. Quadratic fit to the data yielded a K_{10} of 18 ± 9 nM (*solid line*). A fitted curve with K_{10} fixed to 0 (*dashed line*) is shown for comparison. Conditions were as in Fig. 2. *AU*, arbitrary units.

the experiments, it is reasonable to assume that its value is in the nanomolar range, to maintain thermodynamic consistency with the results of the ADP affinity measurements (K_5/K_5

should equal K_{10}/K_6, *cf.* Table I). Thus, ADP binding to NMIIA S1 does not dramatically reduce its actin affinity. This feature is similar to NMIIB and strikingly different from skeletal and cardiac muscle myosins (Table I).

DISCUSSION

The enzymatic properties of myosin II isoforms reflect functional and structural divergence corresponding to their widely differing cellular roles. These functions range from very different speeds of muscle contraction to cortical tension maintenance and contraction of the cytokinetic ring during cell division. It is well known that differential expression of skeletal muscle myosin isoforms is responsible for the greater than 10-fold differences in shortening velocities found among various muscle fiber types (30). Therefore, it is reasonable to assume that the three cytoplasmic myosin isoforms, which are expressed in a tissue- and cell-dependent manner in mammals, also have different functions that are specified by their kinetic properties.

Thus far, there has been little characterization of NMIIC in terms of its cellular distribution and function, but numerous studies have examined the localization of NMIIA and NMIIB within various cultured cell types. In *Xenopus* XTC cells, the two myosins have very different localizations (31). NMIIA is found in stress fibers, whereas NMIIB has a cortical localization. Studies in mammalian cells have shown that although there are regions where the two isoforms are distinctly localized, there is some overlap (10, 32). Both isoforms are usually found in stress fibers, although NMIIB is usually absent from the peripheral regions of these structures. The cortical localization of NMIIB is usually noted in mammalian cells, often near areas of membrane protrusive activity (10). In neuronal cells, NMIIB is the major isoform, and it is concentrated in the growth cone at the marginal region between the organelle-rich central domain and the actin-rich peripheral domain (11). NMIIA is present in much lower amounts and is associated with actin bundles in the central region and the marginal zone.

NMIIA and NMIIB expression have been separately ablated in cultured neuroblastoma cells through the use of antisense oligonucleotides, and an NMIIB knockout mouse has also been produced. Ablation of NMIIB in cultured neuroblastoma cells suppresses neurite outgrowth (33). Similarly, explants cultured from the brains of the NMIIB knockout mice exhibit lower rates of outgrowth, and the growth cones of superior cervical ganglion neurons have altered shape (34, 35). The actin structure within the growth cones of these cells is abnormal, and the filopodia produce less force (34). Many of the NMIIB knockout mouse embryos survive almost until birth, but they exhibit hydrocephaly and have abnormal brain structure suggestive of neural migration defects. Despite observations that both NMIIA and NMIIB localize to the cytokinetic ring of XTC and HeLa cells during mitosis, the *in situ* NMIIB knockout mouse cells obviously carry out cytokinesis in absence of NMIIB as the mouse develops to near term. In contrast, an NMIIA knockout mouse is embryonic lethal at an early stage.[2] The antisense ablation of NMIIA in the neuroblastoma cells leads to a rearrangement of the cytoskeleton and loss of adhesion (36). Thus, in neuroblastoma cells, the two isoforms have very different functions. The predicted ability of NMIIB to dwell in a strongly attached state (8) may be related to the requirement for generating a protrusive force to propel neurite outgrowth.

In terms of sequence similarity, the human non-muscle (or cytoplasmic) myosin II isozymes lie closest to the single smooth muscle myosin isoform of the human genome, which is, interestingly, even more divergent from other muscle myosins (1). This fact is reflected in the kinetic properties of these proteins,

---

[2] M. A. Conti and R. S. Adelstein, personal communication.

although there seems to be no obvious determinant in their primary structure from which the enzymatic parameters could be predicted. A summary of the known kinetic constants of non-muscle and some muscle myosin II S1 constructs is presented in Table I. Besides the generally slow kinetics of virtually all steps of the actoNMIIA S1 ATPase cycle, two main features prompt further discussion. First, the ADP affinity of NMIIA is *not* weakened by actin, as is in the case of muscle myosins. Second, the high ratio of the actoNMIIA S1 ADP release constant and the steady-state ATPase rate indicate a low duty ratio of NMIIA S1.

The ADP affinity of actoNMIIA S1 is slightly greater than that of NMIIA S1 alone ($K_5'/K_5 = 0.7$). The equilibrium constants of actin binding in the absence and presence of ADP indicate that there is no drastic change in affinity of one ligand caused by the other. (The value of K_{10}/K_6, which should equal K_5'/K_5 for thermodynamic consistency, was around 2 in our measurements, although this value contains notable uncertainty.) In this respect, NMIIA S1 is similar to the NMIIB isoform, which has a strong positive coupling between actin and ADP binding, unlike any other myosin assessed previously (Ref. 8 and Table I). Smooth muscle myosin, which has the highest ADP affinity of any muscle myosin in the presence of actin ($K_5' = 5$ μM), still exhibits a 4–5-fold mutual weakening of the affinities.

In terms of rate enhancement of ADP release by actin, NMIIA S1 ($k_5'/k_5 = 2.8$) lies between NMIIB (in which there is indeed a slight opposite effect) and smooth muscle S1 (12-fold enhancement, smallest among muscle myosins). The rate of ADP release from actomyosin is thought to limit the unloaded shortening velocity of muscle (37) and the *in vitro* actin sliding speed (38). An NMIIA heavy meromyosin construct showed a low actin filament sliding velocity of about 0.3 μm/s at 30 °C (7, 39), indicating that actomyosin ADP release may indeed be slow. Consistent with this is the even slower *in vitro* motility rate of NMIIB (<0.1 μm/s at 25 °C) (5).

The rate constant of ADP release from actoNMIIA S1 ($k_5' = 2.2$ s^{-1}) is about 13 times faster than the maximal actin-activated steady-state ATPase rate (0.17 s^{-1}). Our phosphate release measurements indicate that the steady-state ATPase rate is limited by slow phosphate release resulting from low actin affinity of the M·ADP·P$_i$ state (high K_9). The low value of the ATP hydrolysis equilibrium constant ($K_3 = 0.6$) will cause the steady-state K_{ATPase} value to be significantly higher than the K_9 dissociation constant ($K_{ATPase} = K_9(K_3 + 1)/K_3$), but it will not affect the fact that the maximal steady-state ATPase rate is limited by k_4'. Thus, the strong actin-binding AM·ADP state (whose decomposition rate constant is k_5') will probably have a low population during steady-state actomyosin ATP hydrolysis. Indeed, kinetic simulations based on the experimentally determined rate constants indicate that the duty ratio (*i.e.* the fraction of time spent in the strong actin-binding states: AM·ADP plus AM, with the latter having a negligible contribution) will be only about 5% at saturating actin concentration in the absence of an ADP "background," which is elevated only slightly with increasing ADP concentration (to ~11% at 100 μM ADP). Therefore, NMIIA S1 may have a duty ratio that is similar to that measured in muscle myosins (17). This is in contrast to NMIIB S1, in which a moderately high duty ratio (~23–40% in the 0–100 μM ADP concentration range) was indicated based on kinetic constants (8).

Thus, the overall conclusion of the kinetic analysis of NMIIA S1 can be stated as this isoform having a very high actomyosin ADP affinity and low enhancement of the ADP release rate constant by actin, which are also characteristic of NMIIB S1. However, the ADP release rate is still an order of magnitude faster than phosphate release, resulting in a low duty ratio characteristic of muscle myosins, unlike that of NMIIB. The unusual features of NMIIB were proposed to prolong tension maintenance in minifilamentous structures known to exist in the cytoplasm (8, 40). The present study shows that the NMIIA isoform has distinct enzymatic properties, raising also the possibility that myosin cofilaments with heads of multiple types of kinetic "fine tuning" can exist and function in cells. This idea remains to be tested experimentally.

Note Added in Proof—A research paper was published about the kinetic mechanism of non-muscle myosin IIB (Rosenfeld, S. S., Xing, J., Chen, L. Q., and Sweeney, H. L. (2003) *J. Biol. Chem.* **278,** 27449–27455) while this article was being reviewed. Similar to our work on human non-muscle myosin IIB (Ref. 8), the paper of Rosenfeld *et al.* showed elevated duty ratio and high actomyosin ADP affinity of that isoform.

REFERENCES

1. Sellers, J. R. (1999) *Myosins*, 2nd Ed., Oxford University Press, New York
2. De Lozanne, A., and Spudich, J. A. (1987) *Science* **236,** 1086–1091
3. Kong, H. H., and Pollard, T. D. (2002) *J. Cell Sci.* **115,** 4993–5002
4. Berg, J. S., Powell, B. C., and Cheney, R. E. (2001) *Mol. Biol. Cell* **12,** 780–794
5. Pato, M. D., Sellers, J. R., Preston, Y. A., Harvey, E. V., and Adelstein, R. S. (1996) *J. Biol. Chem.* **271,** 2689–2695
6. Umemoto, S., and Sellers, J. R. (1990) *J. Biol. Chem.* **265,** 14864–14869
7. Wang, F., Harvey, E. V., Conti, M. A., Wei, D., and Sellers, J. R. (2000) *Biochemistry* **39,** 5555–5560
8. Wang, F., Kovács, M., Hu, A., Limouze, J., Harvey, E. V., and Sellers, J. R. (2003) *J. Biol. Chem.* **278,** 27439–27448
9. Kawamoto, S., and Adelstein, R. S. (1991) *J. Cell Biol.* **112,** 915–924
10. Maupin, P., Phillips, C. L., Adelstein, R. S., and Pollard, T. D. (1994) *J. Cell Sci.* **107,** 3077–3090
11. Rochlin, M. W., Itoh, K., Adelstein, R. S., and Bridgman, P. C. (1995) *J. Cell Sci.* **108,** 3661–3670
12. Bagshaw, C. R., and Trentham, D. R. (1974) *Biochem. J.* **141,** 331–349
13. Cremo, C. R., and Geeves, M. A. (1998) *Biochemistry* **37,** 1969–1978
14. Lymn, R. W., and Taylor, E. W. (1971) *Biochemistry* **10,** 4617–4624
15. Marston, S. B., and Taylor, E. W. (1980) *J. Mol. Biol.* **139,** 573–600
16. Siemankowski, R. F., and White, H. D. (1984) *J. Biol. Chem.* **259,** 5045–5053
17. Harris, D. E., and Warshaw, D. M. (1993) *J. Biol. Chem.* **268,** 14764–14768
18. Wei, Q., and Adelstein, R. S. (2000) *Mol. Biol. Cell* **11,** 3617–3627
19. Spudich, J. A., and Watt, S. (1971) *J. Biol. Chem.* **246,** 4866–4871
20. Cooper, J. A., Walker, S. B., and Pollard, T. D. (1983) *J. Muscle Res. Cell Motil.* **4,** 253–262
21. Cremo, C. R., Wang, F., Facemyer, K., and Sellers, J. R. (2001) *J. Biol. Chem.* **276,** 41465–41472
22. Konishi, K., Kojima, S., Katoh, T., Yazawa, M., Kato, K., Fujiwara, K., and Onishi, H. (2001) *J. Biochem. (Tokyo)*, 365–372
23. De La Cruz, E. M., Wells, A. L., Rosenfeld, S. S., Ostap, E. M., and Sweeney, H. L. (1999) *Proc. Natl. Acad. Sci. U. S. A.* **96,** 13726–13731
24. De La Cruz, E. M., Ostap, E. M., and Sweeney, H. L. (2001) *J. Biol. Chem.* **276,** 32373–32381
25. Bagshaw, C. R., Eccleston, J. F., Eckstein, F., Goody, R. S., Gutfreund, H., and Trentham, D. R. (1974) *Biochem. J.* **141,** 351–364
26. Malnasi-Csizmadia, A., Pearson, D. S., Kovács, M., Woolley, R. J., Geeves, M. A., and Bagshaw, C. R. (2001) *Biochemistry* **40,** 12727–12737
27. Brune, M., Hunter, J. L., Corrie, J. E., and Webb, M. R. (1994) *Biochemistry* **33,** 8262–8271
28. White, H. D., Belknap, B., and Webb, M. R. (1997) *Biochemistry* **36,** 11828–11836
29. Kurzawa, S. E., and Geeves, M. A. (1996) *J. Muscle Res. Cell Motil.* **17,** 669–676
30. Reggiani, C., Bottinelli, R., and Stienen, G. J. (2000) *News Physiol. Sci.* **15,** 26–33
31. Kelley, C. A., Sellers, J. R., Gard, D. L., Bui, D., Adelstein, R. S., and Baines, I. C. (1996) *J. Cell Biol.* **134,** 675–687
32. Saitoh, T., Takemura, S., Ueda, K., Hosoya, H., Nagayama, M., Haga, H., Kawabata, K., Yamagishi, A., and Takahashi, M. (2001) *FEBS Lett.* **509,** 365–369
33. Wylie, S. R., Wu, P. J., Patel, H., and Chantler, P. D. (1998) *Proc. Natl. Acad. Sci. U. S. A.* **95,** 12967–12972
34. Bridgman, P. C., Dave, S., Asnes, C. F., Tullio, A. N., and Adelstein, R. S. (2001) *J. Neurosci.* **21,** 6159–6169
35. Tullio, A. N., Bridgman, P. C., Tresser, N. J., Chan, C. C., Conti, M. A., Adelstein, R. S., and Hara, Y. (2001) *J. Comp. Neurol.* **433,** 62–74
36. Wylie, S. R., and Chantler, P. D. (2001) *Nat. Cell Biol.* **3,** 88–92
37. Siemankowski, R. F., Wiseman, M. O., and White, H. D. (1985) *Proc. Natl. Acad. Sci. U. S. A.* **82,** 658–662

38. Sellers, J. R., Cuda, G., Wang, F., and Homsher, E. (1993) *Methods Cell Biol.* **39,** 23–49
39. Hu, A., Wang, F., and Sellers, J. R. (2002) *J. Biol. Chem.* **277,** 46512–46517
40. Verkhovsky, A. B., Svitkina, T. M., and Borisy, G. G. (1995) *J. Cell Biol.* **131,** 989–1002
41. Sleep, J. A., and Taylor, E. W. (1976) *Biochemistry* **15,** 5813–5817
42. Wagner, P. D. (1981) *J. Biol. Chem.* **256,** 2493–2498
43. Ritchie, M. D., Geeves, M. A., Woodward, S. K., and Manstein, D. J. (1993) *Proc. Natl. Acad. Sci. U. S. A.* **90,** 8619–8623
44. Millar, N. C., and Geeves, M. A. (1983) *FEBS Lett.* **160,** 141–148
45. Trybus, K. M., and Taylor, E. W. (1982) *Biochemistry* **21,** 1284–1294
46. Bagshaw, C. R., and Trentham, D. R. (1973) *Biochem. J.* **133,** 323–328